Spatial Signatures of Retrograde Spanwise Vortices in Wall Turbulence

By V. K. NATRAJAN[1], Y. WU[1]
AND K. T. CHRISTENSEN[1,2]†

[1]Department of Theoretical and Applied Mechanics, University of Illinois
Urbana, IL 61801, USA

[2]Department of Mechanical and Industrial Engineering, University of Illinois
Urbana, IL 61801, USA

The spatial signatures of retrograde spanwise vortices in wall turbulence are assessed from particle-image velocimetry measurements in the streamwise–wall-normal plane of a zero-pressure-gradient turbulent boundary layer at $\mathrm{Re}_\tau \equiv u_*\delta/\nu = 2350$. The present results suggest that a portion of retrograde spanwise vortices have a well-defined spatial relationship with neighboring prograde vortices. Two-point cross-correlations and conditionally-averaged velocity fields given a retrograde vortex reveal that such structures are typically oriented either upstream/below or downstream/above a prograde core. While the former preferred orientation is consistent with the typical-eddy patterns reported by Falco and co-workers, we offer an alternative interpretation for a portion of these retrograde/prograde pairs. In particular, the arrangement of a retrograde core upstream and below of a prograde core is also consistent with the spatial signature revealed if an omega-shaped hairpin structure were sliced through its shoulder region by a fixed streamwise–wall-normal measurement plane.

1. Introduction

Significant evidence exists supporting the presence of hairpin structures in wall-bounded turbulent flows (Theodorsen 1952; Head & Bandyopadhyay 1981; Smith *et al.* 1991; Zhou *et al.* 1999; Adrian *et al.* 2000; Ganapathisubramani *et al.* 2003, among many others). The observations reported in the latter four efforts also suggest that these vortices align to form larger-scale structures termed vortex packets. These packets are characterized by an inclined interface formed by the heads of the streamwise-aligned vortices as well as a region of large-scale streamwise momentum deficit beneath the interface due to the collective induction of the vortices. When sliced in the streamwise–wall-normal plane, the heads of the individual hairpins appear as spanwise vortex cores with $\omega_z < 0$, where ω_z is the fluctuating spanwise vorticity, and strong ejections of low-speed fluid are observed upstream and below each head due to the collective induction of the hairpin's head and leg(s). Spanwise vortices for which $\omega_z < 0$ are termed prograde spanwise vortices herein since their rotation is in the same sense as the mean shear. Recent efforts by Wu & Christensen (2006) show that the largest populations of prograde spanwise vortices, most of which bear signatures consistent with hairpin heads, occur in the region $y < 0.3\delta$.

Retrograde spanwise vortices, positive ω_z cores, have also been observed in wall turbulence. Falco (1977, 1983, 1991) present evidence of 'typical eddies' in the outer region which bear spatial characteristics consistent with ring-like structures. The flow visual-

† Author to whom correspondence should be addressed: ktc@uiuc.edu

Re_τ	Re_θ	U_∞	δ	θ	u_*	y_*	Δx^+	Δy^+	No. of vectors	No. of
–	–	($\mathrm{m\,s^{-1}}$)	(mm)	(mm)	($\mathrm{m\,s^{-1}}$)	(μm)	–	–	per field	realizations
2350	8330	10.0	103.1	10.1	0.36	43.9	12.3	12.3	34776	2500

TABLE 1. Summary of boundary layer characteristics and experimental parameters.

izations and an idealized schematic of these structures in Falco (1977) show that typical eddies appear as spatially-coincident prograde and retrograde spanwise vortices when sliced in the streamwise–wall-normal plane. Falco (1977, 1983, 1991) offer little discussion regarding a preferred orientation for typical eddies except to state that the idealized schematic in Falco (1977) (which portrays the prograde core above and slightly downstream of the retrograde core) represents the "commonly-observed view" of such a structure in the streamwise–wall-normal plane. More recently, Klewicki & Hirschi (2004) observed that near-wall shear layers often occur in close proximity to clusters of prograde structures as well as adjacent regions of opposing-sign ω_z, with the retrograde event either above or below the prograde event. The generation of ring-like structures may be related to the pinch-off and reconnection of the legs of existing hairpin structures as observed by Moin *et al.* (1986), Smith *et al.* (1991) and Bake *et al.* (2002). Alternatively, Tomkins & Adrian (2003) proposed the generation of isolated retrograde structures via the spanwise merger of hairpin structures. Another possibility is that some fraction of retrograde structures occur in tandem with an adjacent prograde structure via a single, streamwise-aligned hairpin vortex. This latter possibility will be discussed in detail later. Irrespective of their origin, Wu & Christensen (2006) report that retrograde spanwise vortices occur most frequently near $y = 0.2\delta$, with few retrograde structures observed at the inner boundary of the log layer. In addition, the fraction of retrograde structures relative to prograde vortices grows with increasing Reynolds number (Re) in the outer layer, indicating that such structures may play an increasingly important role at higher Re. The present effort documents the spatial signatures of retrograde spanwise vortices and explores their relationship with neighboring prograde cores.

2. Experiment

The experimental data utilized herein is a subset of measurements reported by Wu & Christensen (2006). Two-thousand five-hundred instantaneous velocity (u, v) fields were acquired by particle-image velocimetry (PIV) over a $\delta \times \delta$ field of view in the streamwise–wall-normal $(x - y)$ plane of a zero-pressure-gradient turbulent boundary layer at $\mathrm{Re}_\tau \equiv u_*\delta/\nu = 2350$. The wind-tunnel facility utilized for these measurements has a documented turbulence intensity of 0.16% in the free stream and the boundary layer develops over a 6.1 m-long hydraulically-smooth flat plate (Meinhart 1994). The friction velocity, $u_* = \tau_w/\rho$, and the viscous length scale, $y_* = \nu/u_*$, were determined using the Clauser chart method. The PIV images were interrogated using two-frame cross-correlation methods which yielded nearly thirty-five-thousand vectors per instantaneous velocity field with vector grid spacings in inner units of $\Delta x^+ = \Delta y^+ = 12.3$. Table 2 summarizes the relevant flow parameters and the reader is directed to Wu & Christensen (2006) for further experimental details.

3. Instantaneous Evidence

Determining the spatial characteristics of retrograde vortices requires effective visualization of such structures in the instantaneous velocity realizations. Galilean decomposition of an instantaneous velocity field through removal of a fixed advection velocity reveals vortices advecting at this speed as closed streamline patterns, consistent with the definition of a vortex offered by Kline & Robinson (1989). Galilean decomposition is often most effective when one wishes to visualize the local kinematics induced by vortices but suffers as a global identification tool in situations where the vortex advection velocities have spatial dependence. Alternatively, embedded structure is more efficiently revealed through analysis of the local velocity gradient tensor. One such technique is swirling strength (λ_{ci})–the imaginary part of the complex eigenvalue of the local velocity gradient tensor (Zhou *et al.* 1999). Vortex identification via λ_{ci} is Galilean invariant and does not identify regions of shear that are absent of rotation. While the rotational sense of the swirling motion is not retained in λ_{ci}, one can define

$$\Lambda_{ci}(x,y) = \lambda_{ci}(x,y)\frac{\omega_z(x,y)}{|\omega_z(x,y)|}, \tag{3.1}$$

which assigns the sign of the fluctuating spanwise vorticity to λ_{ci}, facilitating differentiation between prograde ($\Lambda_{ci} < 0$) and retrograde ($\Lambda_{ci} > 0$) spanwise vortices.

Identifying the boundaries of individual vortices using Λ_{ci} requires a suitable threshold. Wu & Christensen (2006) found that a universal swirling-strength threshold, independent of both wall-normal position and Reynolds number, can be achieved through normalization of $\Lambda_{ci}(x,y)$ with its wall-normal-dependent root-mean-square (RMS), $\Lambda_{ci}^{\mathrm{rms}}(y)$ (A similar threshold definition is offered by Nagaosa & Handler (2003) for vortex identification via the second invariant of $\nabla\mathbf{u}$.). A threshold of $|\Lambda_{ci}(x,y)|/\Lambda_{ci}^{\mathrm{rms}}(y) = 1.5$ was found to effectively define the boundaries of vortex cores while minimizing the influence of experimental noise associated with calculation of the velocity gradients (The reader is directed to Wu & Christensen (2006) for a more complete discussion of this methodology). Both Galilean decomposition and Λ_{ci} with the aforementioned threshold are employed herein to study the spatial signatures of retrograde spanwise vortices.

Figure 1(a) presents a representative Galilean-decomposed instantaneous velocity field in the streamwise–wall-normal plane of a turbulent boundary layer at $\mathrm{Re}_\tau = 2350$ with an advection velocity of $0.81U_\infty$ removed. The instantaneous Λ_{ci} field associated with this velocity realization is presented as figure 1(b). Several prograde and retrograde spanwise vortices are visible in the Galilean decomposition, each of which has a cluster of non-zero Λ_{ci} associated with it. In addition, several additional Λ_{ci} clusters are noted at locations where swirling motions are not observed in the Galilean decomposition. Five streamwise-aligned prograde vortices (labeled A–E) are noted near $(x,y) = (0.25\delta, 0.1\delta)$ with each vortex exhibiting a strong ejection of fluid away from the wall just below and upstream of its core. These spatial characteristics are consistent with the hairpin vortex signature offered by Adrian *et al.* (2000), indicating that these prograde spanwise vortices are likely the heads of hairpin vortices. In addition, these vortices form a tent-like interface and a large-scale region of streamwise momentum deficit is observed below this interface due to the collective induction of the vortices, consistent with the hairpin-packet observations of Adrian *et al.* (2000).

In addition to these hairpin structures, two retrograde vortices are also revealed in the Galilean-decomposed velocity field (labeled F and G). The insets to figure 1(a) present zoomed-in views of the local velocity fields around these two retrograde vortices, with each visualized retrograde structure appearing in close proximity to a prograde vortex just

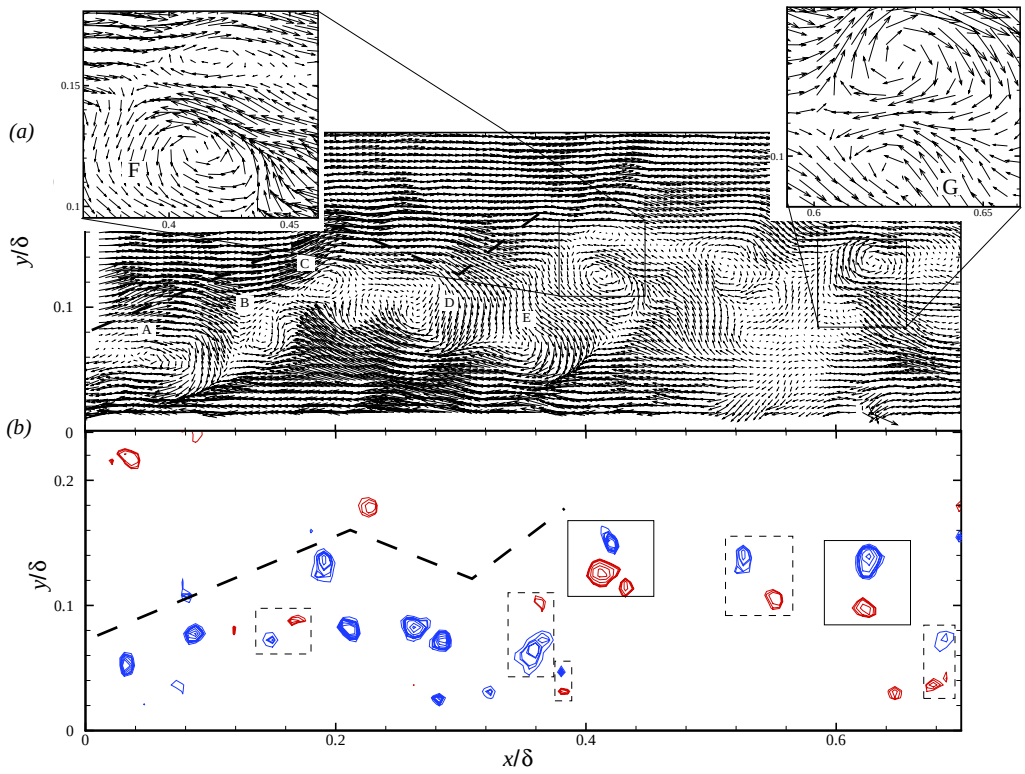

FIGURE 1. (a) Galilean-decomposed velocity field in the streamwise–wall-normal plane. (b) Retrograde (red) and prograde (blue) Λ_{ci} calculated from the velocity field in (a).

above and upstream of its core. While a few isolated retrograde structures are apparent in the Λ_{ci} field, a majority of the retrograde structures appear in close proximity to prograde cores in various orientations. These possible pairings are highlighted in figure 1(b) in dashed-line bounding boxes with the orientation of a retrograde core upstream and below a prograde core observed most often. In contrast, many of the prograde vortices occur in isolation rather than in tandem with retrograde structures.

4. Statistical Evidence

4.1. *Two-point correlations*

Two-point spatial correlations between the swirling strengths of prograde and retrograde vortices are calculated to further explore the spatial characteristics of retrograde cores, particularly their relationship with neighboring prograde vortices. To facilitate this calculation, each instantaneous Λ_{ci} field is divided into a prograde field as

$$\Lambda^{p}_{ci}(x,y) = \begin{cases} \Lambda_{ci}(x,y) & \text{if } \Lambda_{ci}(x,y) \leqslant -1.5\Lambda^{\mathrm{rms}}_{ci}(y), \\ 0 & \text{otherwise.} \end{cases} \tag{4.1}$$

and a retrograde field as

$$\Lambda^{r}_{ci}(x,y) = \begin{cases} \Lambda_{ci}(x,y) & \text{if } \Lambda_{ci}(x,y) \geqslant +1.5\Lambda^{\mathrm{rms}}_{ci}(y), \\ 0 & \text{otherwise.} \end{cases} \tag{4.2}$$

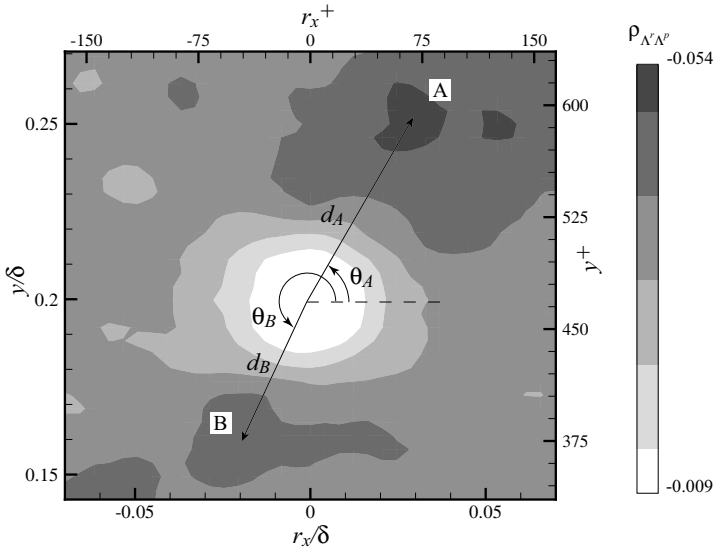

FIGURE 2. Two-point cross-correlation coefficient between Λ_{ci}^r and Λ_{ci}^p, $\rho_{\Lambda^r\Lambda^p}$, at $y_{\rm ref} = 0.2\delta$.

using the aforementioned threshold. This decomposition yields efficient separation of prograde and retrograde cores and facilitates calculation of a two-point cross-correlation coefficient of the form

$$\rho_{\Lambda^r\Lambda^p}(r_x, y) = \frac{\langle \Lambda_{ci}^r(x, y_{\rm ref})\Lambda_{ci}^p(x + r_x, y)\rangle}{\sigma_{\Lambda^r}(y_{\rm ref})\sigma_{\Lambda^p}(y)}, \tag{4.3}$$

where σ_{Λ^r} and σ_{Λ^p} are the root-mean-squares of Λ_{ci}^r and Λ_{ci}^p, respectively. These correlation coefficients are computed over all 2500 statistically-independent realizations to minimize statistical sampling errors.

Figure 2 presents $\rho_{\Lambda^r\Lambda^p}$ at $y_{\rm ref} = 0.2\delta$, the wall-normal location where the largest populations of retrograde vortices are found (Wu & Christensen 2006). The cross-correlation coefficient is zero at the event location and negative elsewhere, as expected, since we are cross-correlating retrograde swirl with prograde swirl The cross-correlation coefficient displays two regions of significant correlation that represent preferred orientations of prograde structures relative to retrograde cores. The first region is observed downstream and above the event location $(r_x, y) = (0, y_{\rm ref})$ and its peak is denoted 'A' in figure 2. The second region of significant correlation (labeled 'B') is weaker than the first and appears upstream and below of the event location. These orientations can be quantified by a radial distance from the event location, d, and an angle relative to horizontal, θ, yielding $d_A^+ = 135$ ($d_A = 0.058\delta$) and $\theta_A = 65°$ for peak location A and $d_B^+ = 103.5$ ($d_B = 0.044\delta$) and $\theta_B = 230°$ for peak location B. However, it should be noted that both regions of correlation span a rather broad angular range: $30° < \theta_A < 90°$ and $210° < \theta_B < 290°$.

4.2. *Spatial orientations of neighboring retrograde and prograde vortices*

Given the preferred spatial orientations of prograde vortices relative to retrograde cores observed in $\rho_{\Lambda^r\Lambda^p}$, we explore this relationship further by considering histograms of the spacing (d) and angular orientation (θ) of instantaneous, spatially-coincident retrograde and prograde vortices. Each retrograde vortex at $y = 0.2\delta$ in the instantaneous Λ_{ci} fields is identified, its closest prograde neighbor is determined and the spacing and angular orientation of the prograde core relative to the retrograde vortex are then assessed.

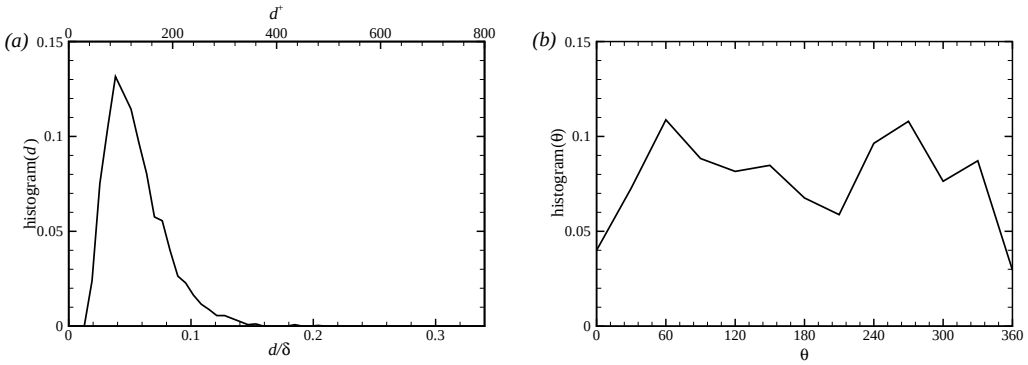

FIGURE 3. Histograms of (a) spacing, d, and (b) angular orientation, θ, between identified retrograde vortices at $y = 0.2\delta$ and their closest prograde neighbors.

Figures 3(a) and 3(b) present histograms of d and θ, respectively, at $y = 0.2\delta$. The peak in the distance histogram occurs near $d^+ = 100$ $(= 0.042\delta)$ while broad peaks in the angle histogram occur over the ranges $40 < \theta < 90°$ and $220° < \theta < 280°$, consistent with the character of $\rho_{\Lambda^r\Lambda^p}$.

4.3. *Conditionally-averaged velocity fields*

Conditionally-averaged velocity fields given the presence of a retrograde vortex are also computed to uncover their average velocity signature. These averages are accomplished by centering a bounding box of width and height 0.2δ around each identified retrograde vortex at $y = 0.2\delta$ and the local velocity field contained within this box is extracted. The instantaneous advection velocity of each identified retrograde vortex is removed, yielding the local velocity field in the reference frame of the identified retrograde vortex. Since $\rho_{\Lambda^r\Lambda^p}$ (figure 2) and the histogram of angular orientation (figure 3(b)) demonstrate clear orientation preferences between retrograde and prograde structures, the identified retrograde vortices are sorted into four ensembles based upon the angular orientation of their closest prograde neighbor: $0° \leqslant \theta < 90°$, $90° \leqslant \theta < 180°$, $180° \leqslant \theta < 270°$ and $270° \leqslant \theta < 360°$. Conditional averages are then computed for each subset.

Figure 4(a–d) presents conditionally-averaged velocity fields for retrograde vortices centered at $y = 0.2\delta$ computed for each of the angular subsets outlined above. We first consider the conditionally-averaged velocity field for a retrograde spanwise vortex whose closest prograde neighbor resides in the range $0° \leqslant \theta < 90°$. This subset constitutes 26% of the total number of identified retrograde vortices at $y = 0.2\delta$ (1401 retrograde vortices total) and the corresponding conditionally-averaged velocity field presented in figure 4(a) reveals a well-defined prograde vortex oriented downstream and above the retrograde core at an angle of approximately 47° and spacing of $103y_*$ $(= 0.044\delta)$. This orientation is consistent with the character of both $\rho_{\Lambda^r\Lambda^p}$ and the histograms of spacing and angular orientation. This spatial signature is also quite consistent with the local velocity fields associated with the two identified retrograde structures presented as insets to figure 1(a). Taken together, these observations indicate a clear preference for some retrograde vortices at $y = 0.2\delta$ to be oriented below and upstream of prograde cores.

The conditionally-averaged velocity field for the angular range $180° \leqslant \theta < 270°$ is presented as figure 4(c). Recall that both $\rho_{\Lambda^r\Lambda^p}$ and the histograms of angular orientation indicate a preference for this angular range. The retrograde samples included in this average comprise roughly 26% of the retrograde vortices at $y = 0.2\delta$ and the conditional average reveals a well-defined prograde vortex below and upstream of the retrograde core

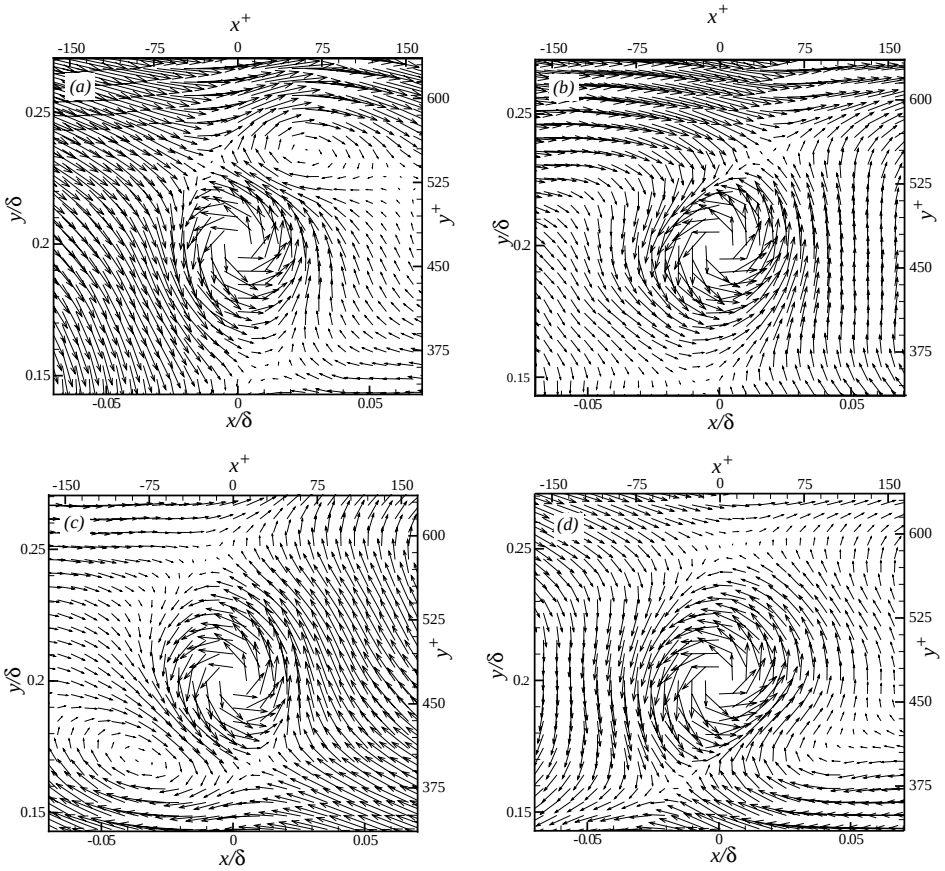

FIGURE 4. Conditionally averaged velocity fields given a retrograde vortex at $y = 0.2\delta$ for which the closest prograde vortex is oriented (a) $0^\circ \leqslant \theta < 90^\circ$, (b) $90^\circ \leqslant \theta < 180^\circ$, (c) $180^\circ \leqslant \theta < 270^\circ$ and (d) $270^\circ \leqslant \theta < 360^\circ$ relative to the retrograde core.

with a relative spacing of 0.046δ ($= 108y_*$) at an angle of 220°. Finally, the $90^\circ \leqslant \theta < 180^\circ$ (figure 4(b)) and $270^\circ \leqslant \theta < 360^\circ$ (figure 4(d)) ensembles, which account for 25% and 23% of the retrograde vortices at $y = 0.2\delta$, respectively, reveal average velocity fields devoid of prograde vortices.

While the conditionally-averaged velocity fields in figure 4 indicate that retrograde vortices are often related to neighboring prograde vortices oriented in the ranges $0^\circ \leqslant \theta < 90^\circ$ and $180^\circ \leqslant \theta < 270^\circ$, it is not clear whether the opposite case is true. That is, do a majority of prograde vortices occur in tandem with neighboring retrograde structures? The instantaneous example presented in figure 1 suggests no, but a more definitive answer to this question is achieved by considering the average velocity field given the presence of a prograde vortex. As with the retrograde conditional averages, prograde vortices at a given wall-normal location are separated into four ensembles based on their orientation relative to their closest retrograde neighbor. A bounding box is centered about the core of each prograde vortex and the velocity field in the reference frame of the prograde core is extracted. Figure 5(a–d) presents conditionally-averaged velocity fields given a prograde vortex at $y = 0.2\delta$ for prograde structures oriented in the ranges $0^\circ \leqslant \theta < 90^\circ$, $90^\circ \leqslant \theta < 180^\circ$, $180^\circ \leqslant \theta < 270^\circ$ and $270^\circ \leqslant \theta < 360^\circ$, respectively, relative to their closest retrograde neighbors. Each of these conditionally-averaged prograde structures displays

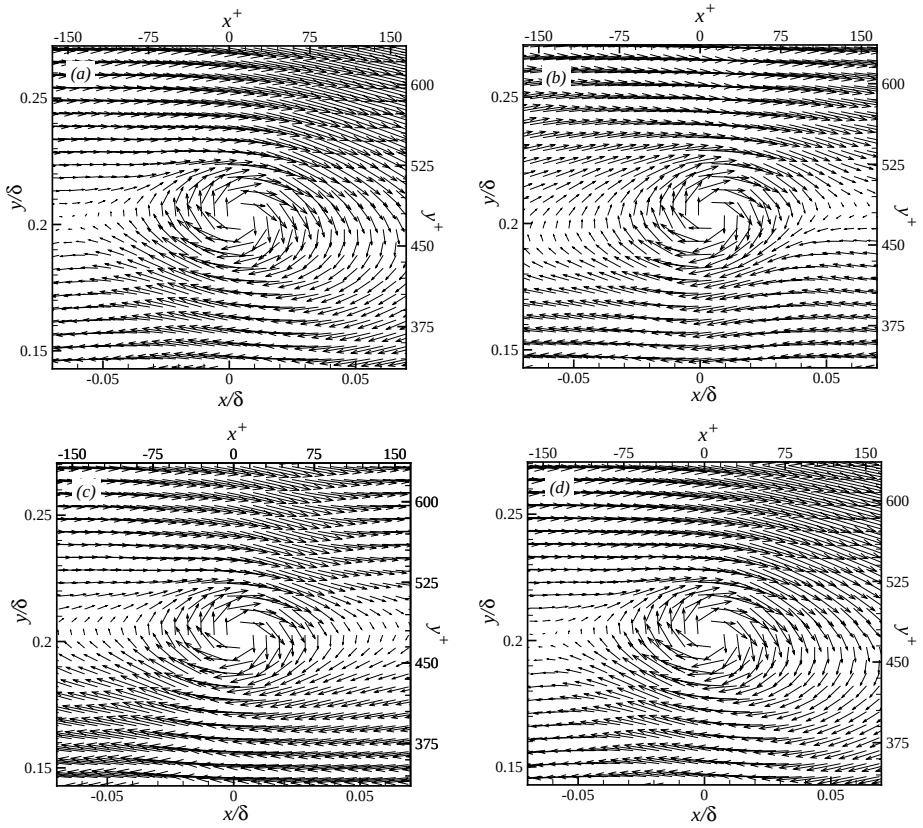

FIGURE 5. Conditionally averaged velocity fields given a prograde vortex at $y = 0.2\delta$ oriented (a) $0^\circ \leqslant \theta < 90^\circ$, (b) $90^\circ \leqslant \theta < 180^\circ$, (c) $180^\circ \leqslant \theta < 270^\circ$ and (d) $270^\circ \leqslant \theta < 360^\circ$ relative to its closest retrograde neighbor.

a closed streamline pattern with clockwise rotation and a strong ejection of low-speed fluid away from the wall, consistent with the hairpin vortex signature offered by Adrian *et al.* (2000). Of further significance is the fact that none of these conditionally-averaged fields reveals a neighboring retrograde vortex. Therefore, while many retrograde cores are related to a neighboring prograde vortex, the opposite is not true: a vast majority of prograde spanwise vortices in and around the log layer occur in isolation rather than in tandem with neighboring retrograde structures.

5. Conclusions

Instantaneous evidence is presented indicating a spatial relationship between retrograde and prograde spanwise vortices near the outer edge of the log layer where the retrograde populations are largest (Wu & Christensen 2006). The present results suggest that many retrograde vortices occur in tandem with neighboring prograde cores with angular orientations $40^\circ < \theta < 90^\circ$ and $220^\circ < \theta < 290^\circ$ (relative to the retrograde cores) and a mean spacing of approximately $100y_*$. These characteristics are observed in spatial cross-correlations of retrograde and prograde swirling strength, histograms of the spacing and angular orientation between identified retrograde vortex cores and their closest prograde neighbor as well as conditional averages of the local velocity field around iden-

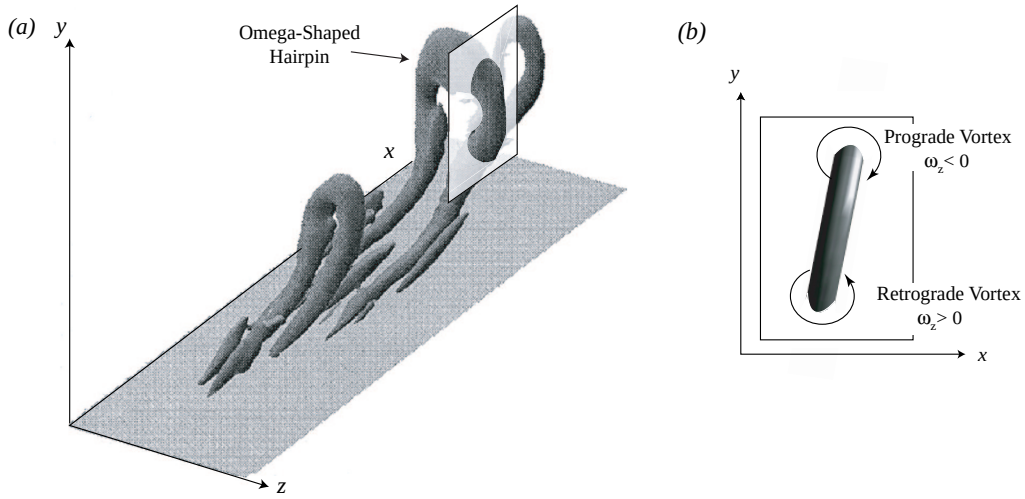

FIGURE 6. (a) Three-dimensional visualization of a hairpin vortex packet adapted from Zhou *et al.* (1999) illustrating the existence of omega-shaped hairpin structures. (b) Spatial signature revealed if the omega-shaped structure in (a) were sliced through one of its shoulders in the streamwise–wall-normal plane.

tified retrograde vortices. Further, the preferred alignment of retrograde vortices either above or below prograde cores is consistent with the orientations of adjacent regions of opposing-sign ω_z observed in the vicinity of near-wall shear layers by Klewicki & Hirschi (2004). In contrast, many prograde spanwise vortices occur in isolation.

The spatial relationships between retrograde and prograde spanwise vortices reported herein are certainly not inconsistent with the flow-visualization observations of spatially-coincident prograde and retrograde cores by Falco and co-workers. As noted earlier, Falco (1977, 1983, 1991) present many flow visualizations and schematics of spatially-coincident prograde and retrograde vortex cores in the streamwise–wall-normal plane, nearly always with the prograde core oriented above and downstream of the retrograde core. This arrangement is consistent with one of the preferred orientations presented herein. However, an alternate argument for this orientation preference can be made by supposing that some fraction of these spatially-coincident prograde and retrograde cores are actually related to one-another through a single, streamwise-aligned hairpin structure. Evidence supporting this possibility has been presented in the literature (Zhou *et al.* 1999; Bake *et al.* 2002, for example); however, this specific argument for the origin of some fraction of retrograde vortices has not yet been proposed.

Figure 6(a) presents a three-dimensional visualization of a vortex packet reported in Zhou *et al.* (1999) that illustrates the possible development of hairpin structures with distinct omega shapes around their shoulders and heads (adapted from figure 3(c) in Zhou *et al.* (1999)). Similar omega-shaped structures are also presented in Bake *et al.* (2002). If the omega-shaped hairpin in figure 6(a) were sliced in the streamwise–wall-normal plane through its spanwise center, a single prograde spanwise vortex associated with the head of the hairpin would be observed. If, however, this structure were sliced through either of its shoulders, two spanwise vortices would be revealed as illustrated in figure 6(b): one with clockwise rotation (a prograde structure) above and downstream of a second vortex core with counterclockwise rotation (a retrograde vortex). This spatial signature is consistent with the patterns presented in the insets of figure 1(a) and the conditionally-averaged velocity field of figure 4(a). The possibility of slicing through the

shoulder of an omega-shaped hairpin on occasion in a fixed streamwise–wall-normal flow visualization or PIV measurement is certainly a reasonable one given that a preferred spanwise alignment of such structures relative to a fixed measurement plane cannot be expected. Further, this alternate explanation is not inconsistent with the observations of Falco and co-workers since significant evidence exists that hairpins can, under certain conditions, pinch off at their legs and reconnect to form ring-like structures (Moin *et al.* 1986; Smith *et al.* 1991; Bake *et al.* 2002). The presence of ring-like vortices generated in this manner would then account for observations of prograde/retrograde pairs with alternate angular orientations, including the secondary orientation of a retrograde vortex above and downstream of a prograde core observed herein.

This work was performed with funding from the Air Force Office of Scientific Research under Grants FA9550-05-1-0043 and FA9550-05-1-0246 (Dr. Rhett Jeffries, Program Manager) and the University of Illinois.

REFERENCES

Adrian, R. J., Meinhart, C. D. & Tomkins, C. D. 2000 Vortex organization in the outer region of the turbulent boundary layer. *J. Fluid Mech.* **422**, 1–54.

Bake, S., Meyer, G. W. & Rist, U. 2002 Turbulence mechanism in Klebanoff transition: A quantitative comparison of experiment and direct numerical simulation. *J. Fluid Mech.* **459**, 217–243.

Falco, R. E. 1977 Coherent motions in the outer region of turbulent boundary layers. *Phys. Fluids* **20** (10), S124–S132.

Falco, R. E. 1983 New results, a review and synthesis of the mechanism of turbulence production in boundary layers and its modification. In *AIAA Paper 83-0377*.

Falco, R. E. 1991 A coherent structure model of the turbulent boundary layer and its ability to predict Reynolds number dependence. *Phil. Trans. R. Soc. Lond. A* **336**, 103–129.

Ganapathisubramani, B., Longmire, E. K. & Marusic, I. 2003 Characteristics of vortex packets in turbulent boundary layers. *J. Fluid Mech.* **478**, 35–46.

Head, M. R. & Bandyopadhyay, P. 1981 New aspects of turbulent boundary-layer structure. *J. Fluid Mech.* **107**, 297–338.

Klewicki, J. C. & Hirschi, C. R. 2004 Flow field properties local to near-wall shear layers in a low Reynolds number turbulent boundary layer. *Phys. Fluids* **16** (11), 4163–4176.

Kline, S. J. & Robinson, S. K. 1989 Quasi-coherent structures in the turbulent boundary layer. Part 1: Status report on a community-wide summary of the data. In *Near Wall Turbulence* (ed. S. J. Kline & N. H. Afgan), pp. 218–247. Hemisphere.

Meinhart, C. D. 1994 Investigation of turbulent boundary-layer structure using particle-image velocimetry. PhD thesis, Department of Theoretical and Applied Mechanics, University of Illinois at Urbana-Champaign, Urbana, Ill.

Moin, P., Leonard, A. & Kim, J. 1986 Evolution of a curved vortex filament into a vortex ring. *Phys. Fluids* **29**, 955–963.

Nagaosa, R. & Handler, R. A. 2003 Statistical analysis of coherent vortices near a free surface in a fully developed turbulence. *Phys. Fluids* **15** (2), 375–394.

Smith, C. R., Walker, J. D. A., Haidari, A. H. & Sobrun, U. 1991 On the dynamics of near-wall turbulence. *Philosophical Transactions of the Royal Society of London A* **336**, 131–175.

Theodorsen, T. 1952 Mechanism of turbulence. In *Proceedings of the 2nd Midwestern Conference on Fluid Mechanics*, pp. 1–19. Ohio State University, Columbus, Ohio.

Tomkins, C. D. & Adrian, R. J. 2003 Spanwise structure and scale growth in turbulent boundary layers. *J. Fluid Mech.* **490**, 37–74.

Wu, Y. & Christensen, K. T. 2006 Population trends of spanwise vortices in wall turbulence. *J. Fluid Mech.* Submitted.

Zhou, J., Adrian, R. J., Balachandar, S. & Kendall, T. M. 1999 Mechanisms for generating coherent packets of hairpin vortices in channel flow. *J. Fluid Mech.* **387**, 353–396.

List of Recent TAM Reports

No.	Authors	Title	Date
1009	Bagchi, P., and S. Balachandar	Effect of turbulence on the drag and lift of a particle—*Physics of Fluids*, in press (2003)	Oct. 2002
1010	Zhang, S., R. Panat, and K. J. Hsia	Influence of surface morphology on the adhesive strength of aluminum/epoxy interfaces—*Journal of Adhesion Science and Technology* **17**, 1685–1711 (2003)	Oct. 2002
1011	Carlson, D. E., E. Fried, and D. A. Tortorelli	On internal constraints in continuum mechanics—*Journal of Elasticity* **70**, 101–109 (2003)	Oct. 2002
1012	Boyland, P. L., M. A. Stremler, and H. Aref	Topological fluid mechanics of point vortex motions—*Physica D* **175**, 69–95 (2002)	Oct. 2002
1013	Bhattacharjee, P., and D. N. Riahi	Computational studies of the effect of rotation on convection during protein crystallization—*International Journal of Mathematical Sciences* **3**, 429–450 (2004)	Feb. 2003
1014	Brown, E. N., M. R. Kessler, N. R. Sottos, and S. R. White	*In situ* poly(urea-formaldehyde) microencapsulation of dicyclopentadiene—*Journal of Microencapsulation* (submitted)	Feb. 2003
1015	Brown, E. N., S. R. White, and N. R. Sottos	Microcapsule induced toughening in a self-healing polymer composite—*Journal of Materials Science* (submitted)	Feb. 2003
1016	Kuznetsov, I. R., and D. S. Stewart	Burning rate of energetic materials with thermal expansion—*Combustion and Flame* (submitted)	Mar. 2003
1017	Dolbow, J., E. Fried, and H. Ji	Chemically induced swelling of hydrogels—*Journal of the Mechanics and Physics of Solids*, in press (2003)	Mar. 2003
1018	Costello, G. A.	Mechanics of wire rope—Mordica Lecture, Interwire 2003, Wire Association International, Atlanta, Georgia, May 12, 2003	Mar. 2003
1019	Wang, J., N. R. Sottos, and R. L. Weaver	Thin film adhesion measurement by laser induced stress waves—*Journal of the Mechanics and Physics of Solids* (submitted)	Apr. 2003
1020	Bhattacharjee, P., and D. N. Riahi	Effect of rotation on surface tension driven flow during protein crystallization—*Microgravity Science and Technology* **14**, 36–44 (2003)	Apr. 2003
1021	Fried, E.	The configurational and standard force balances are not always statements of a single law—*SIAM Journal on Applied Mathematics* **66**, 1130–1149 (2006)	Apr. 2003
1022	Panat, R. P., and K. J. Hsia	Experimental investigation of the bond coat rumpling instability under isothermal and cyclic thermal histories in thermal barrier systems—*Proceedings of the Royal Society of London A* **460**, 1957–1979 (2003)	May 2003
1023	Fried, E., and M. E. Gurtin	A unified treatment of evolving interfaces accounting for small deformations and atomic transport: grain-boundaries, phase transitions, epitaxy—*Advances in Applied Mechanics* **40**, 1–177 (2004)	May 2003
1024	Dong, F., D. N. Riahi, and A. T. Hsui	On similarity waves in compacting media—*Horizons in World Physics* **244**, 45–82 (2004)	May 2003
1025	Liu, M., and K. J. Hsia	Locking of electric field induced non-180° domain switching and phase transition in ferroelectric materials upon cyclic electric fatigue—*Applied Physics Letters* **83**, 3978–3980 (2003)	May 2003
1026	Liu, M., K. J. Hsia, and M. Sardela Jr.	In situ X-ray diffraction study of electric field induced domain switching and phase transition in PZT-5H—*Journal of the American Ceramics Society* (submitted)	May 2003
1027	Riahi, D. N.	On flow of binary alloys during crystal growth—*Recent Research Development in Crystal Growth* **3**, 49–59 (2003)	May 2003
1028	Riahi, D. N.	On fluid dynamics during crystallization—*Recent Research Development in Fluid Dynamics* **4**, 87–94 (2003)	July 2003
1029	Fried, E., V. Korchagin, and R. E. Todres	Biaxial disclinated states in nematic elastomers—*Journal of Chemical Physics* **119**, 13170–13179 (2003)	July 2003
1030	Sharp, K. V., and R. J. Adrian	Transition from laminar to turbulent flow in liquid filled microtubes—*Physics of Fluids* (submitted)	July 2003

List of Recent TAM Reports (cont'd)

No.	*Authors*	*Title*	*Date*
1031	Yoon, H. S., D. F. Hill, S. Balachandar, R. J. Adrian, and M. Y. Ha	Reynolds number scaling of flow in a Rushton turbine stirred tank: Part I—Mean flow, circular jet and tip vortex scaling—*Chemical Engineering Science* (submitted)	Aug. 2003
1032	Raju, R., S. Balachandar, D. F. Hill, and R. J. Adrian	Reynolds number scaling of flow in a Rushton turbine stirred tank: Part II—Eigen-decomposition of fluctuation—*Chemical Engineering Science* (submitted)	Aug. 2003
1033	Hill, K. M., G. Gioia, and V. V. Tota	Structure and kinematics in dense free-surface granular flow—*Physical Review Letters* **91**, 064302 (2003)	Aug. 2003
1034	Fried, E., and S. Sellers	Free-energy density functions for nematic elastomers—*Journal of the Mechanics and Physics of Solids* **52**, 1671–1689 (2004)	Sept. 2003
1035	Kasimov, A. R., and D. S. Stewart	On the dynamics of self-sustained one-dimensional detonations: A numerical study in the shock-attached frame—*Physics of Fluids* (submitted)	Nov. 2003
1036	Fried, E., and B. C. Roy	Disclinations in a homogeneously deformed nematic elastomer—*Nature Materials* (submitted)	Nov. 2003
1037	Fried, E., and M. E. Gurtin	The unifying nature of the configurational force balance—*Mechanics of Material Forces* (P. Steinmann and G. A. Maugin, eds.), 25–32 (2005)	Dec. 2003
1038	Panat, R., K. J. Hsia, and J. W. Oldham	Rumpling instability in thermal barrier systems under isothermal conditions in vacuum—*Philosophical Magazine*, in press (2004)	Dec. 2003
1039	Cermelli, P., E. Fried, and M. E. Gurtin	Sharp-interface nematic–isotropic phase transitions without flow—*Archive for Rational Mechanics and Analysis* **174**, 151–178 (2004)	Dec. 2003
1040	Yoo, S., and D. S. Stewart	A hybrid level-set method in two and three dimensions for modeling detonation and combustion problems in complex geometries—*Combustion Theory and Modeling* (submitted)	Feb. 2004
1041	Dienberg, C. E., S. E. Ott-Monsivais, J. L. Ranchero, A. A. Rzeszutko, and C. L. Winter	Proceedings of the Fifth Annual Research Conference in Mechanics (April 2003), TAM Department, UIUC (E. N. Brown, ed.)	Feb. 2004
1042	Kasimov, A. R., and D. S. Stewart	Asymptotic theory of ignition and failure of self-sustained detonations—*Journal of Fluid Mechanics* (submitted)	Feb. 2004
1043	Kasimov, A. R., and D. S. Stewart	Theory of direct initiation of gaseous detonations and comparison with experiment—*Proceedings of the Combustion Institute* (submitted)	Mar. 2004
1044	Panat, R., K. J. Hsia, and D. G. Cahill	Evolution of surface waviness in thin films via volume and surface diffusion—*Journal of Applied Physics* (submitted)	Mar. 2004
1045	Riahi, D. N.	Steady and oscillatory flow in a mushy layer—*Current Topics in Crystal Growth Research*, in press (2004)	Mar. 2004
1046	Riahi, D. N.	Modeling flows in protein crystal growth—*Current Topics in Crystal Growth Research*, in press (2004)	Mar. 2004
1047	Bagchi, P., and S. Balachandar	Response of the wake of an isolated particle to isotropic turbulent cross-flow—*Journal of Fluid Mechanics* (submitted)	Mar. 2004
1048	Brown, E. N., S. R. White, and N. R. Sottos	Fatigue crack propagation in microcapsule toughened epoxy—*Journal of Materials Science* (submitted)	Apr. 2004
1049	Zeng, L., S. Balachandar, and P. Fischer	Wall-induced forces on a rigid sphere at finite Reynolds number—*Journal of Fluid Mechanics* (submitted)	May 2004
1050	Dolbow, J., E. Fried, and H. Ji	A numerical strategy for investigating the kinetic response of stimulus-responsive hydrogels—*Computer Methods in Applied Mechanics and Engineering* **194**, 4447–4480 (2005)	June 2004
1051	Riahi, D. N.	Effect of permeability on steady flow in a dendrite layer—*Journal of Porous Media*, in press (2004)	July 2004

List of Recent TAM Reports (cont'd)

No.	*Authors*	*Title*	*Date*
1052	Cermelli, P., E. Fried, and M. E. Gurtin	Transport relations for surface integrals arising in the formulation of balance laws for evolving fluid interfaces—*Journal of Fluid Mechanics* **544**, 339–351 (2005)	Sept. 2004
1053	Stewart, D. S., and A. R. Kasimov	Theory of detonation with an embedded sonic locus—*SIAM Journal on Applied Mathematics* (submitted)	Oct. 2004
1054	Stewart, D. S., K. C. Tang, S. Yoo, M. Q. Brewster, and I. R. Kuznetsov	Multi-scale modeling of solid rocket motors: Time integration methods from computational aerodynamics applied to stable quasi-steady motor burning—*Proceedings of the 43rd AIAA Aerospace Sciences Meeting and Exhibit* (January 2005), Paper AIAA-2005-0357 (2005)	Oct. 2004
1055	Ji, H., H. Mourad, E. Fried, and J. Dolbow	Kinetics of thermally induced swelling of hydrogels—*International Journal of Solids and Structures* **43**, 1878–1907 (2006)	Dec. 2004
1056	Fulton, J. M., S. Hussain, J. H. Lai, M. E. Ly, S. A. McGough, G. M. Miller, R. Oats, L. A. Shipton, P. K. Shreeman, D. S. Widrevitz, and E. A. Zimmermann	Final reports: Mechanics of complex materials, Summer 2004 (K. M. Hill and J. W. Phillips, eds.)	Dec. 2004
1057	Hill, K. M., G. Gioia, and D. R. Amaravadi	Radial segregation patterns in rotating granular mixtures: Waviness selection—*Physical Review Letters* **93**, 224301 (2004)	Dec. 2004
1058	Riahi, D. N.	Nonlinear oscillatory convection in rotating mushy layers—*Journal of Fluid Mechanics*, in press (2005)	Dec. 2004
1059	Okhuysen, B. S., and D. N. Riahi	On buoyant convection in binary solidification—*Journal of Fluid Mechanics* (submitted)	Jan. 2005
1060	Brown, E. N., S. R. White, and N. R. Sottos	Retardation and repair of fatigue cracks in a microcapsule toughened epoxy composite—Part I: Manual infiltration—*Composites Science and Technology* (submitted)	Jan. 2005
1061	Brown, E. N., S. R. White, and N. R. Sottos	Retardation and repair of fatigue cracks in a microcapsule toughened epoxy composite—Part II: *In situ* self-healing—*Composites Science and Technology* (submitted)	Jan. 2005
1062	Berfield, T. A., R. J. Ong, D. A. Payne, and N. R. Sottos	Residual stress effects on piezoelectric response of sol-gel derived PZT thin films—*Journal of Applied Physics* (submitted)	Apr. 2005
1063	Anderson, D. M., P. Cermelli, E. Fried, M. E. Gurtin, and G. B. McFadden	General dynamical sharp-interface conditions for phase transformations in viscous heat-conducting fluids—*Journal of Fluid Mechanics* (submitted)	Apr. 2005
1064	Fried, E., and M. E. Gurtin	Second-gradient fluids: A theory for incompressible flows at small length scales—*Journal of Fluid Mechanics* (submitted)	Apr. 2005
1065	Gioia, G., and F. A. Bombardelli	Localized turbulent flows on scouring granular beds—*Physical Review Letters*, in press (2005)	May 2005
1066	Fried, E., and S. Sellers	Orientational order and finite strain in nematic elastomers—*Journal of Chemical Physics* **123**, 044901 (2005)	May 2005
1067	Chen, Y.-C., and E. Fried	Uniaxial nematic elastomers: Constitutive framework and a simple application—*Proceedings of the Royal Society of London A* **462**, 1295–1314 (2006)	June 2005
1068	Fried, E., and S. Sellers	Incompatible strains associated with defects in nematic elastomers—*Journal of Chemical Physics* **124**, 024908 (2006)	Aug. 2005
1069	Gioia, G., and X. Dai	Surface stress and reversing size effect in the initial yielding of ultrathin films—*Journal of Applied Mechanics*, in press (2005)	Aug. 2005
1070	Gioia, G., and P. Chakraborty	Turbulent friction in rough pipes and the energy spectrum of the phenomenological theory—*Physical Review Letters* **96**, 044502 (2006)	Aug. 2005

List of Recent TAM Reports (cont'd)

No.	*Authors*	*Title*	*Date*
1071	Keller, M. W., and N. R. Sottos	Mechanical properties of capsules used in a self-healing polymer—*Experimental Mechanics* (submitted)	Sept. 2005
1072	Chakraborty, P., G. Gioia, and S. Kieffer	Volcán Reventador's unusual umbrella	Sept. 2005
1073	Fried, E., and S. Sellers	Soft elasticity is not necessary for striping in nematic elastomers—*Journal of Applied Physics*, in press (2006)	Sept. 2005
1074	Fried, E., M. E. Gurtin, and Amy Q. Shen	Theory for solvent, momentum, and energy transfer between a surfactant solution and a vapor atmosphere—*Physical Review E*, in press (2006)	Sept. 2005
1075	Chen, X., and E. Fried	Rayleigh–Taylor problem for a liquid–liquid phase interface—*Journal of Fluid Mechanics* (submitted)	Oct. 2005
1076	Riahi, D. N.	Mathematical modeling of wind forces—In *The Euler Volume* (Abington, UK: Taylor and Francis), in press (2005)	Oct. 2005
1077	Fried, E., and R. E. Todres	Mind the gap: The shape of the free surface of a rubber-like material in the proximity to a rigid contactor—*Journal of Elasticity* **80**, 97–151 (2005)	Oct. 2005
1078	Riahi, D. N.	Nonlinear compositional convection in mushy layers—*Journal of Fluid Mechanics* (submitted)	Dec. 2005
1079	Bhattacharjee, P., and D. N. Riahi	Mathematical modeling of flow control using magnetic fluid and field—In *The Euler Volume* (Abington, UK: Taylor and Francis), in press (2005)	Dec. 2005
1080	Bhattacharjee, P., and D. N. Riahi	A hybrid level set/VOF method for the simulation of thermal magnetic fluids—*International Journal for Numerical Methods in Engineering* (submitted)	Dec. 2005
1081	Bhattacharjee, P., and D. N. Riahi	Numerical study of surface tension driven convection in thermal magnetic fluids—*Journal of Crystal Growth* (submitted)	Dec. 2005
1082	Riahi, D. N.	Inertial and Coriolis effects on oscillatory flow in a horizontal dendrite layer—*Transport in Porous Media* (submitted)	Jan. 2006
1083	Wu, Y., and K. T. Christensen	Population trends of spanwise vortices in wall turbulence—*Journal of Fluid Mechanics* (submitted)	Jan. 2006
1084	Natrajan, V. K., and K. T. Christensen	The role of coherent structures in subgrid-scale energy transfer within the log layer of wall turbulence—*Physics of Fluids* (submitted)	Jan. 2006
1085	Wu, Y., and K. T. Christensen	Reynolds-stress enhancement associated with a short fetch of roughness in wall turbulence—*AIAA Journal* (submitted)	Jan. 2006
1086	Fried, E., and M. E. Gurtin	Cosserat fluids and the continuum mechanics of turbulence: A generalized Navier–Stokes-α equation with complete boundary conditions—*Journal of Fluid Mechanics* (submitted)	Feb. 2006
1087	Riahi, D. N.	Inertial effects on rotating flow in a porous layer—*Journal of Porous Media* (submitted)	Feb. 2006
1088	Li, F., and D. E. Leckband	Dynamic strength of adhesion surfaces—*Journal of Chemical Physics* (submitted)	Mar. 2006
1089	Chen, X., and E. Fried	Squire's theorem for the Rayleigh–Taylor problem with a phase transformation—*Proceedings of the Royal Society of London A* (submitted)	Mar. 2006
1090	Kim, T.-Y., J. Dolbow, and E. Fried	A numerical method for a second-gradient theory of incompressible fluid flow—*Journal of Computational Physics* (submitted)	Apr. 2006
1091	Natrajan, V. K., Y. Wu, and K. T. Christensen	Spatial signatures of retrograde spanwise vortices in wall turbulence—*Journal of Fluid Mechanics* (submitted)	Apr. 2006